The Role of Long-Term Trends in Seasonal Predictions: Implication of Global Warming in the NCEP CFS

MING CAI AND CHUL-SU SHIN

Department of Meteorology, The Florida State University, Tallahassee, Florida

H. M. VAN DEN DOOL AND WANQIU WANG

NOAA/NWS/NCEP/Climate Prediction Center, Camp Springs, Maryland

S. SAHA

NOAA/NWS/NCEP/Environmental Modeling Center, Camp Springs, Maryland

A. KUMAR

NOAA/NWS/NCEP/Climate Prediction Center, Camp Springs, Maryland

(Manuscript received 14 November 2008, in final form 17 February 2009)

ABSTRACT

This paper analyzes long-term surface air temperature trends in a 25-yr (1982–2006) dataset of retrospective seasonal climate predictions made by the NCEP Climate Forecast System (CFS), a model that has its atmospheric greenhouse gases fixed at the 1988 concentration level. Although the CFS seasonal forecasts tend to follow the observed interannual variability very closely, there exists a noticeable time-dependent discrepancy between the CFS forecasts and observations, with a warm model bias before 1988 and a cold bias afterward except for a short-lived warm bias during 1992–94. The trend from warm to cold biases is likely caused by not including the observed increase in the anthropogenic greenhouse gases in the CFS, whereas the warm bias in 1992–94 reflects the absence of the anomalous aerosols released by the 1991 Mount Pinatubo eruption. Skill analysis of the CFS seasonal climate predictions with and without the warming trend suggests that the 1997–98 El Niño event contributes significantly to the record-breaking global warmth in 1998 whereas the record-breaking warm decade since 2000 is mainly due to the effects of the increased greenhouse gases. Implications for operational seasonal prediction will be discussed.

1. Introduction

Traditionally, operational *weather* forecast centers have not paid much attention to changing greenhouse gases (GHG). In a 2-week forecast this may seem acceptable at first thought. Indeed, the National Centers for Environmental Prediction (NCEP) Global Forecast System as of 2008 still employed a 1988 GHG concentration, so the need for updating GHGS in the model apparently must have seemed low (an update is planned for 2009). In most cases short-term *climate* prediction (or long-range weather prediction as it used to be called) is the outgrowth of technology employed originally for numerical weather prediction so the earliest of such climate prediction efforts neglected to address changing GHGs. Currently, few operational weather and climate forecast centers use coupled climate models with time-evolving GHG concentrations for their operational seasonal climate predictions. The assumption behind such a configuration, other than tradition, is that the global warming signal contained in the initial conditions will largely remain unchanged during the forecast target period, which typically ranges from a few days to several months to one year at most.

As of 2008, the years 1998, 2005, and 2007 ranked as the warmest three years and the average of the last 10 years (1998–2007) is the warmest decade in the instrumental

Corresponding author address: Huug van den Dool, NOAA/NWS/NCEP/Climate Prediction Center, 5200 Auth Rd., Camp Springs, MD 20746.
E-mail: huug.vandendool@noaa.gov

DOI: 10.1175/2009WAF2222231.1

record of global mean surface air temperatures since 1850 (Trenberth et al. 2007; Levinson and Lawrimore 2008; Hansen et al. 2007). The multidecade-long Intergovernmental Panel on Climate Change climate simulations, which do change GHGs, suggest that the record-breaking global warmth in the last decade is a continuation of the upward warming trend observed since the mid–twentieth century in response to the increase of GHGs (Hegerl et al. 2007; Hoerling et al. 2007; Solomon et al. 2007). However, the warming trend may not be captured by climate models for seasonal climate predictions because of the usage of a constant and outdated concentration of GHGs. This omission is becoming one of the main factors contributing to cold biases in the seasonal forecasts of the global mean surface temperature (Doblas-Reyes et al. 2006; Liniger et al. 2007). In practice, the operationally issued public seasonal predictions attempt to take the warming trend into consideration by employing empirical tools, such as the optimal climate normal method (Huang et al. 1996) as used at the Climate Prediction Center (CPC) since the mid-1990s. Climate trends as expressed by optimal climate normals (OCN) have come to dominate real-time U.S. seasonal prediction over the last 10 years. The fundamental questions are to what extent the global warming signal is lost in the seasonal dynamical forecast with constant GHG concentration and what are the impacts of the loss of global warming on seasonal forecast skill, even on a regional scale? Essentially, the issue at hand is whether we need to do dynamical seasonal predictions with a climate model as an initial-value (including ocean!) problem subject to the influence of increasing GHGs (Smith et al. 2007).

In this study, we analyze the 25-yr (1982–2006) retrospective seasonal climate predictions made recently by NCEP's Climate Forecast System (CFS), which has a constant GHG concentration fixed at the 1988 level (Saha et al. 2006), and compare the CFS forecasts to their initial conditions, which are (a) the NCEP–Department of Energy Atmospheric Model Intercomparison Project (AMIP-II) reanalysis (R-2) data (Kanamitsu et al. 2002) for the atmosphere and land and (b) the Global Ocean Data Assimilation System (GODAS) for the ocean (Behringer and Xue 2004). We will focus on the analysis of the decay of the global warming signal in 2-m surface air temperature (SAT) with forecast lead time and explore the potential of seasonal climate predictability arising from the long-term warming trend. Note that we do not have a set of model forecasts that includes the GHG effect. Having such runs available would allow us to, as did Doblas-Reyes et al. (2006) and Liniger et al. (2007), compare model states with and without GHG increases. Instead, we compare reality (subject to GHG increases) to model states with constant GHGs but realistic initial states.

Our analysis can also be considered as an alternate way to reveal the effects of anthropogenic GHGs. The advantage of this alternative method is that, by virtue of including the warming signal in the initial conditions, this approach could isolate anomalies in individual years that are due to the natural variability of the climate system from the response to anthropogenic GHGs, provided that the climate models for dynamical seasonal forecasts have a relatively good level of skill for high-frequency interannual natural climate variability.

2. Some technical details

The atmospheric component of the CFS is the NCEP Global Forecast System with a spectral truncation of 62 waves (T62) in the horizontal plane (equivalent to nearly a 200-km grid) and a finite differencing in the vertical direction with 64 layers. The oceanic component is the Geophysical Fluid Dynamics Laboratory Modular Ocean Model, version 3 (MOM3; Pacanowski and Griffies 1998). The domain of MOM3 is quasi global, extending from 74°S to 64°N. The atmospheric and oceanic components are coupled without any flux adjustment. Full interaction between atmospheric and oceanic components is confined to 65°S–50°N. Poleward of 74°S and 64°N, SSTs experienced by the atmospheric component are taken from the observed climatology. Between 74° and 65°S, and between 64° and 50°N, SSTs for the atmospheric component are the weighted average of the observed climatology and that from MOM3. Sea ice extent is prescribed from the observed climatology.

For each initial month, 15 ensemble forecast members were produced by the CFS for forecasts with lead times from 1 through 9 months. As described in Saha et al. (2006), the 15 members are produced by starting integrations from the 5 days surrounding the 0000 UTC states on the 1st, 11th, the 21st days of the previous month. The ensemble mean of the 15 forecast members for each of the nine monthly lead times is regarded as a monthly CFS forecast. We organize the monthly forecasts with the same lead time into a time series of 25-yr monthly forecasts based on their verification times (month and year). Together with the monthly mean SAT fields derived from the R-2 (which are referred to as observations), we have a total of 10 time series of monthly SAT fields (1 from the observations and the remaining 9 from the monthly forecasts with lead times of 1–9 months). For each of the 10 monthly time series, the yearly mean fields are obtained by averaging across 12 calendar months within the same year, which gives rise to 10 time series of annual means for the period of 1982–2006. The yearly

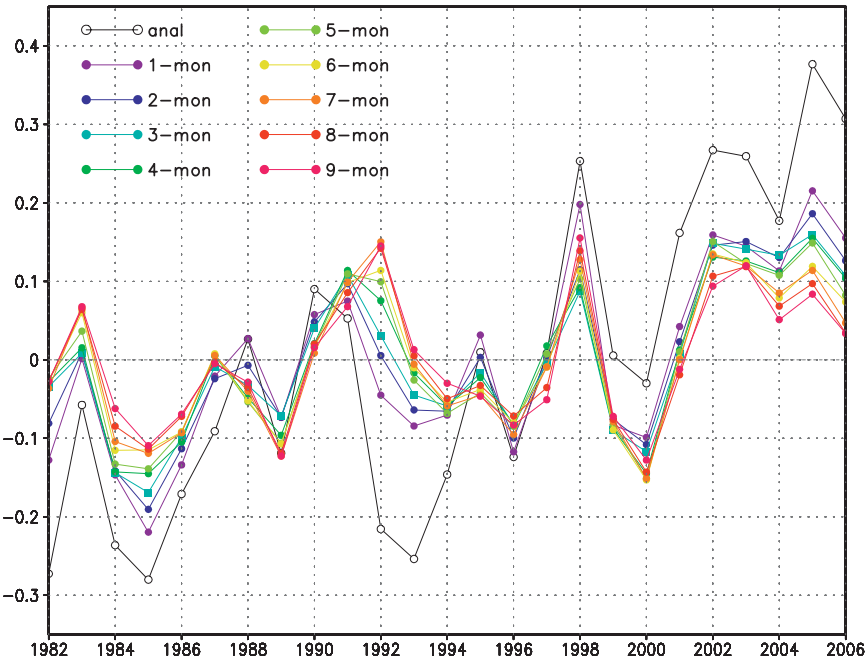

FIG. 1. The time series of the global average SAT anomalies (°C) of observations or R-2 analysis (black) and CFS forecasts at various lead times (colors). Anomalies are relative to the 1982–2006 mean.

anomalies of forecasts and observations are taken as the departures from their corresponding 25-yr averages.

We are aware that the trends in R-2 have been questioned because (i) very few surface data are assimilated and (ii) the model component of the data assimilation system does not have the temporally increasing GHGs as do the observations. However, the theoretical work by Cai and Kalnay (2005) shows that a reanalysis system could recover the trend present in the assimilated observations even if the model component of the reanalysis system has a constant concentration of GHGs. Nevertheless, the reanalysis trend could be somewhat smaller than the trend in the observations. To assess the deficiency of the trend in the R-2 initial states used by the CFS model, we therefore have also compared R-2 with the Global Historical Climatology Network–Climate Anomaly Monitoring System (GHCN–CAMS) global *land* surface air temperature analysis (Fan and Van den Dool 2008). It is found that the warming trend averaged over global land between 64°S and 64°N using the R-2 [0.24 K $(10\ \text{yr})^{-1}$] is about one-third weaker than in the GHCN–CAMS [0.36 K $(10\ \text{yr})^{-1}$], but keep in mind that this comparison applies over land only.

3. Results

Figure 1 compares the time series of the yearly and global mean anomalies of SAT derived from the R-2 (i.e., the initial conditions for the CFS forecasts) and the ensemble mean of CFS forecasts with lead time ranging from 1 to 9 months. The black line in Fig. 1 shows the R-2's gradual upward trend in global mean SAT, with potent interannual variations superimposed. It is evident that the CFS forecasts at all of the nine lead times tend to follow both the upward trend and the observed higher-frequency ups and downs throughout the 25-yr period, implying that the CFS is capable of capturing the dominant signal of the interannual variability of the yearly global mean SAT anomalies. However, there exists a noticeable time-dependent discrepancy between the CFS forecasts and the observations. It is seen that whereas the global mean SAT anomalies in the CFS forecasts tend to be warmer than the observations before 1988, the CFS is colder than the observations afterward (except briefly between 1992 and 1994, during which time the CFS forecasts are warmer than the observations by as much as 0.35°C). Such a discrepancy between the CFS forecasts and the observations is consistent with the lack of a temporally evolving atmospheric composition in the CFS. Specifically, the warm bias (relative to R-2) in the CFS forecasts prior to 1988 coincides with the excessive amount of GHG concentration specified in the CFS hindcasts. The warm bias in the CFS forecasts during 1992–94 overlaps with the period of the temporary global cooling in 1992–94 that was due to the anomalous aerosols released from the 1991 Mount Pinatubo eruption

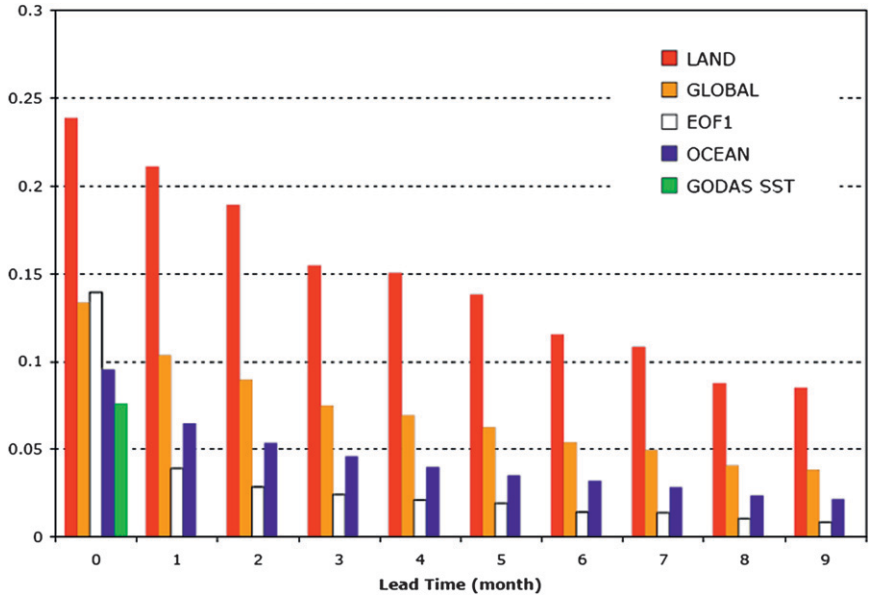

FIG. 2. Linear trends of the SAT anomalies [°C (10 yr)$^{-1}$] averaged over 64°S and 64°N derived from observations or analysis (lead time of 0) and from the CFS forecasts (lead time of 1–9 months). Global: all grids between 64°S and 64°N; land: all land grids between 64°S and 64°N; ocean: all ocean grids over 64°S and 64°N; EOF1: the temperature trend is derived from the R-2-derived EOF1 pattern shown in Fig. 4a, below. The green histogram, for lead time of 0 only, represents the upper ocean, i.e., is based on water temperatures at 5-m depth as analyzed in GODAS.

(Hansen et al. 1992). The cold bias (relative to R-2) in the CFS forecasts after 1994, on the other hand, appears to be associated with the insufficient GHGs in the CFS model, which remained fixed at the 1988 concentration level out to 2006. Figure 1 also shows that the discrepancy between the CFS forecasts and R-2-based observations is more pronounced at a longer lead time. This is consistent with the lack of the evolving atmospheric composition in the CFS that would lead to a larger bias as the forecast lead time increases because whatever the CFS ''knows'' about global warming comes only from the information contained in the time series of its initial conditions, and this information is not maintained during the forecast.

Here, one may question whether the model drift influences the trends as shown in Fig. 1. Although there is significant model drift, we believe that we have eliminated that drift from the estimate of the model's climate trend by organizing the model data by fixed forecast leads; that is, all forecasts at the same lead time are suffering from the same amount of drift when calculating the trend.

As mentioned above, in addition to the constant GHG concentration fixed at the 1988 level, the sea surface temperatures (SST) over the region poleward of 74°S and 64°N in the CFS were taken from the observed climatology instead of being predicted. As a result, the lack of the warming trend in the region poleward of 74°S and 64°N in the CFS forecasts cannot, with certainty, be attributed to the CFS's fixed GHG concentration level only. For this reason, in Fig. 2, we only show the linear trends obtained by averaging data over the domain between 64°S and 64°N. It is seen that the global SAT, derived from the R-2, has a linear warming trend of about 0.14°C (10 yr)$^{-1}$ from 1982 to 2006, which is consistent with other estimates (Trenberth et al. 2007). The warming over land in R-2 [about 0.24°C (10 yr)$^{-1}$] is more than 2 times as large as that seen in SAT over the ocean [about 0.095°C (10 yr)$^{-1}$]. Clearly, the CFS forecasts cannot maintain the warming trends seen in the initial conditions. The warming trends in the CFS forecasts diminish rapidly as the forecast lead time increases, consistent with the fixed GHG concentration in the CFS model, but they have not disappeared completely at 9-month lead time. In terms of the global mean SAT, the warming trend in the CFS forecasts at 9-month lead time is less than one-third (29%) of that in the initial conditions. Another important feature, very surprising perhaps, is that the fading of the warming trend in the CFS forecasts with lead time is faster over the ocean (despite its high thermal capacity) than that over land. At the 9-month lead time, the warming trend

over the ocean in the CFS forecasts is only about one-quarter (22.5%) of that in the initial conditions, whereas the warming trend over land in the CFS forecasts is still about one-third (35.6%) of the land warming trend in the initial conditions. Figure 2 also shows that the warming trend in the ocean initial conditions as estimated from GODAS [about 0.076°C $(10\ \text{yr})^{-1}$] is nearly as large as that of the SAT over the ocean. This essentially rules out the possibility that the rapid diminishment of the SAT warming trend in the CFS forecasts over the oceans is due to the lack of a warming trend in the ocean initial conditions produced by GODAS in the CFS. This further strengthens our conjecture that the fading of the warming trend initially present in the CFS is due to the absence of the time-evolving GHG concentration in the CFS. Our results are broadly consistent with recent findings obtained with the European Centre for Medium-Range Weather Forecasts coupled seasonal forecast model (Doblas-Reyes et al. 2006; Liniger et al. 2007).

We next evaluate the skill of the CFS seasonal climate forecasts using the traditional map anomaly correlation (AC) between the SAT anomalies in the observations and the CFS forecasts with and without the global warming trend signal present. Shown in Fig. 3a is the AC of the CFS forecasts of the yearly SAT anomalies as a function of the verification time and the lead time. It is seen that the CFS forecasts have remarkably high skill at all nine of the lead times in the years between 1982 and 1989 and between 1996 and 2000 (the left-top panel in Fig. 3). On average, the CFS forecasts have good skill (AC > 0.4) up to the 5-month lead time (the right panel in Fig. 3a). For later reference, 95% confidence error bars are shown (in all right-hand panels of Fig. 3) around the AC die-off curve. The error bars are based on assuming 50 degrees of freedom for temperature on a global domain [see Van den Dool and Chervin (1986) for such estimates]. To explore to what extent the skill of the CFS forecasts in Fig. 3a has benefited from the global warming signal in the initial conditions, we examine the CFS forecasts under two hypothetical situations: one with (experiment ''as is'') and the other without (by filtering) the global warming trend. We use empirical orthogonal function (EOF) analysis to isolate the spatial pattern of the global warming signal from the interannual variability in the annual mean SAT anomaly field. It turns out that it is only the first EOF mode, which is derived from global R-2 data (shown in Fig. 4), and which explains about 30% of the total variance of the yearly mean SAT anomalies between 1982 and 2006, that exhibits a pronounced upward trend (Fig. 4b). The reconstructed global mean observed SAT associated with just the first EOF yields an upward trend of about 0.145°C $(10\ \text{yr})^{-1}$, which is nearly identical to the global warming trend derived from the whole dataset (the white-colored vs orange-colored bars in Fig. 2 at the initial time). The spatial pattern of the global warming mode (Fig. 4a) exhibits a familiar warming pattern, showing a larger warming in high latitudes and over land as documented in the literature (Trenberth et al. 2007). We have also verified that the pattern shown in Fig. 4a is very similar to the difference between the averages of 1997–2006 and 1981–1992 (not shown here), suggesting that the pattern in Fig. 4a is representative of the global warming pattern.

We construct the dataset for the first hypothetical situation in which both the observations and CFS forecasts would have the global warming signal removed by

$$\text{SAT}^{\text{no-trend}}(s, t; \tau) = \text{SAT}(s, t; \tau) - \alpha(\tau)(t - 1988) \times \text{EOF}_1(s), \quad (1)$$

where s and t denote spatial location and time (t runs from 1982 to 2006), τ is the forecast lead time ($\tau = 0$ corresponds to the initial state and $\tau = n$ corresponds to the n-month lead time for $n = 1, 2, \ldots, 9$), $\text{EOF}_1(s)$ is the observed global warming pattern shown in Fig. 4a, and $\alpha(\tau)$ is the linear trend portion of the projection of $\text{SAT}(s, t; \tau)$ onto $\text{EOF}_1(s)$ [e.g., $\alpha(\tau = 0)$ corresponds to both the slope of the red line in Fig. 4b *and* the height of the white colored bar in Fig. 2]. In the second hypothetical situation, we consider a hypothetical climate model that otherwise would be identical to the CFS model except that it would capture the observed global warming pattern exactly (a perfect trend model). The ''forecasts'' of the hypothetical ''perfect trend model'' are constructed according to

$$\text{SAT}^{\text{perfect-trend}}(s, t; \tau) = \text{SAT}(s, t; \tau) + [\alpha(\tau = 0) - \alpha(\tau)](t - 1988) \times \text{EOF}_1(s), \quad (2)$$

where all of the notations on the right-hand side of Eq. (2) are identical to those in Eq. (1). Obviously, the procedure in Eq. (2) should have no effect on the data for lead 0, or in 1988 for any lead. This implies that the 1988 AC skills in these two hypothetical situations are identical to what is shown in Fig. 3a. The choice of 1988 implicitly assumes that the CFS forecasts made in 1988 would not suffer the biases caused by the lack of the updated GHG concentration because the CFS's GHGs are kept at the 1988 level. We have also used different years instead of 1988 and found that the basic characteristics of the results shown in Figs. 3b and 3c remain unchanged.

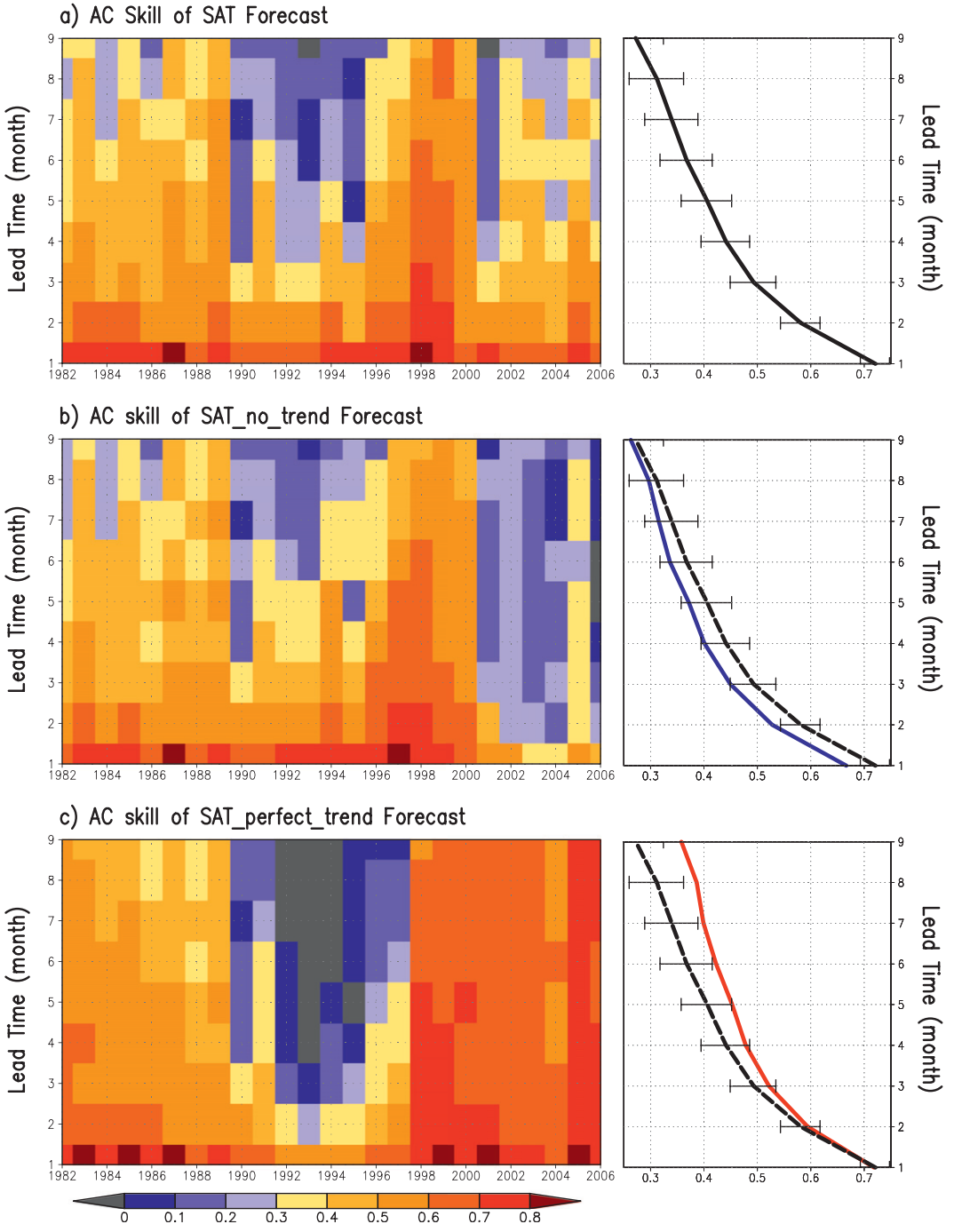

FIG. 3. The AC skill of the forecasts as a function of the verification time (abscissa, year) and lead time (ordinate, month). The panels on the right show the AC skill averaged over all 25 yr. (a) CFS forecasts; (b) hypothetical forecasts using Eq. (1); (c) hypothetical forecasts using Eq. (2). The dashed curves in the right-hand panels of (b) and (c) correspond to the curve in the right-hand panel of (a). The 95% confidence bars are shown around the AC die-off curve in all right-hand panels.

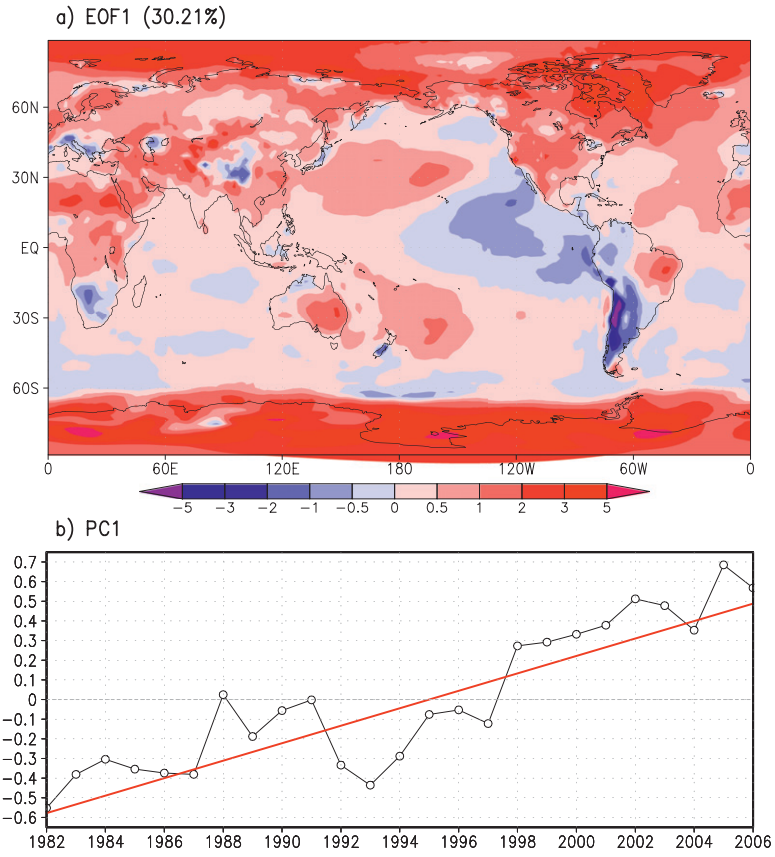

FIG. 4. The first EOF mode of the yearly SAT anomalies in R-2: (a) the spatial pattern and (b) the time series of the first EOF mode (black; the red curve is its linear trend). The units are arbitrary, but the product of EOF and the time series yields degrees Celsius.

It is shown in Fig. 3b that the skill of the ''no trend'' CFS forecasts at all of the nine lead times (verified against ''detrended'' observations) is nearly as good as that of the actual CFS forecasts against the total observed anomaly that includes the trend (Fig. 3a) in the years from 1982 to 2000 but becomes noticeably worse after 2000. The comparable level of skill shown in Figs. 3a and 3b before 2001 implies that the skill of the CFS forecasts mainly comes from the CFS's ability to capture interannual variability, such as the El Niño/La Niña events in 1982/82, 1986/87, 1988/89, 1991/92, and 1997/98 (Wang et al. 2005). The warming-trend signal in the initial conditions contributes only a little to the skill of the CFS forecasts prior to 2000. Because both Figs. 3a and 3b show relatively poor skill in the period of 1992–95, the main reason of the poor skill in this period is likely the absence (in the CFS model) of the anomalous aerosols released from the 1991 Mount Pinatubo eruption. The noticeable downturn in skill between 2001 and 2006 in Fig. 3b suggests that the skill of the CFS forecasts in this period shown in Fig. 3a is because the warming signal in the initial conditions is maintained into the forecast. It is also the lack of large-amplitude El Niño/La Niña events between 2001 and 2006 that causes a somewhat poor performance of the CFS in this period because apart from the global warming signal in the initial conditions the CFS's seasonal climate prediction skill has to come mainly from its ability to capture the ENSO signal (Wang et al. 2005).

In Fig. 3c, we plot the AC of the hypothetical perfect-trend model, constructed using Eq. (2). In comparison with Fig. 3a, the inclusion of the perfect global warming signal in the CFS forecasts would have improved the forecasts significantly in most years, but especially and suddenly post-1998. The average AC skill of the CFS seasonal climate forecasts would still be above 0.3 at the 9-month lead should the CFS model capture the linear part of the global warming trend exactly. If we exclude the years between 1992 and 1995, the average AC of the hypothetical perfect-trend model is as high as 0.45 at

9-month lead time. Furthermore, because the CFS's original forecasts in 1997/98 are already very good (AC > 0.5 at 8-month lead time), the further improvement of the seasonal forecast skill by including the full-strength global warming signal suggests that both the 1997/98 El Niño event and the anthropogenic GHGs together contribute to the record-breaking global warmth in 1998. In contrast, the record-breaking global warmth since 2001 is more likely due to the direct impact of increasing GHGs because without the updated GHGs and in the absence of the large-amplitude El Niño/La Niña events, the CFS has little skill in the years between 2001 and 2006.

What we see, with reference to the die-off curves on the rhs of Fig. 3, is that taking out the model's trend (cf. Figs. 3a and 3b), imperfect as it may be, reduces the skill on average, and more significantly so at short leads. What we see next (cf. Figs. 3c and 3b) is that inserting the observed linear trend into the model forecast improves the skill, and more significantly so at the longer leads. This all makes perfect sense.

4. Conclusions

Our analysis suggests that an adequate representation of the anthropogenic GHGs in coupled climate models for seasonal forecasts has become essential for more accurate seasonal climate predictions, even at the regional level. While climate trends may be present in the initial state of models with fixed GHGs, this trend erodes to 30% in about 9 months, as revealed by studying a set of 25 years of hindcasts by NCEP's CFS model. Surprisingly, the warming trend in surface air temperature over the ocean is lost just as fast (if not faster) than over land. The official National Weather Service seasonal predictions have recognized the impact of global warming on the seasonal forecast skill a long time ago and introduced an empirical trend tool [called optimal climate normals by Huang et al. (1996)] to explicitly take the warming trend into consideration in the seasonal climate predictions released by CPC. The inclusion of temporally evolving GHGs is planned at NCEP for the next CFS (accompanied by new hindcasts back to 1982) in 2010. Nevertheless, a set of seasonal climate predictions made with a fixed concentration of GHGs, if affordable, would still be useful and might actually help in determining the association between individual extreme events (a severe heat wave, a drought event, or a record-breaking global warmth year) and the increase in GHGs.

Although this paper has ostensibly been about seasonal prediction, the problem of climate change, observed temperature trends, and GHG touches obviously upon much longer time scales than the 9-month predictions made by the CFS model. Indeed, seasonal to interannual forecasts are linked to decadal forecasts (e.g., Cox and Stephenson 2007) and could be made by the same technology, whether it be a model like CFS (with increasing GHGs) or empirical methods like OCN (Huang et al. 1996).

Acknowledgments. This work is supported in part by NOAA CPO Grants GC06-038 and GC08-292.

REFERENCES

Behringer, D. W., and Y. Xue, 2004: Evaluation of the Global Ocean Data Assimilation System at NCEP: The Pacific Ocean. Preprints, *Eighth Symp. on Integrated Observing and Assimilation Systems for Atmosphere, Oceans, and Land Surface,* Seattle, WA, Amer. Meteor. Soc., 2.3. [Available online at http://ams.confex.com/ams/pdfpapers/70720.pdf.]

Cai, M., and E. Kalnay, 2005: Can reanalysis have anthropogenic climate trends without model forcing? *J. Climate,* **18,** 1844–1849.

Cox, P., and D. Stephenson, 2007: A changing climate for prediction. *Science,* **317,** 207–208, doi:10.1126/science.1145956.

Doblas-Reyes, F. J., R. Hagedorn, T. N. Palmer, and J.-J. Morcrette, 2006: Impact of increasing greenhouse gas concentration in seasonal ensemble forecasts. *Geophys. Res. Lett.,* **33,** L07708, doi:10.1029/2005GL025061.

Fan, Y., and H. Van den Dool, 2008: A global monthly land surface air temperature analysis for 1948–present. *J. Geophys. Res.,* **113,** D01103, doi:10.1029/2007JD008470.

Hansen, J., A. Lacis, R. Ruedy, and M. Sato, 1992: Potential climate impact of Mount Pinatubo eruption. *Geophys. Res. Lett.,* **19,** 215–218.

——, and Coauthors, cited 2007: GISS 2007 temperature analysis. [Available online at http://www.columbia.edu/~jeh1/mailings/20080114_GISTEMP.pdf.]

Hegerl, G. C., and Coauthors, 2007: Understanding and attributing climate change. *Climate Change 2007: The Physical Science Basis,* S. Solomon et al., Eds., Cambridge University Press, 663–745.

Hoerling, M., J. Eischeid, X. Quan, and T. Xu, 2007: Explaining the record U.S. warmth of 2006. *Geophys. Res. Lett.,* **34,** L17704, doi:10.1029/2007GL030643.

Huang, J., H. Van den Dool, and A. G. Barnston, 1996: Long-lead seasonal temperature prediction using optimal climate normals. *J. Climate,* **9,** 809–817.

Kanamitsu, M., W. Ebisuzaki, J. Woollen, S.-K. Yang, J. J. Hnilo, M. Fiorino, and G. L. Potter, 2002: NCEP–DOE AMIP-II reanalysis (R-2). *Bull. Amer. Meteor. Soc.,* **83,** 1631–1643.

Levinson, D. H., and J. H. Lawrimore, 2008: State of the climate in 2007. *Bull. Amer. Meteor. Soc.,* **89** (7), S1–S179.

Liniger, M. A., H. Mathis, C. Appenzeller, and F. J. Doblas-Reyes, 2007: Realistic greenhouse gas forcing and seasonal forecasts. *Geophys. Res. Lett.,* **34,** L04705, doi:10.1029/2006GL028335.

Pacanowski, R. C., and S. M. Griffies, 1998: MOM 3.0 manual. NOAA/Geophysical Fluid Dynamics Laboratory Tech. Rep. 4, 680 pp.

Saha, S., and Coauthors, 2006: The NCEP Climate Forecast System. *J. Climate,* **19,** 3483–3517.

Smith, D. M., S. Cusack, A. W. Colman, C. K. Folland, G. R. Harris, and J. M. Murphy, 2007: Improved surface temperature prediction for the coming decade from a global climate model. *Science,* **317,** 796–799, doi:10.1126/science.1139540.

Solomon, S., and Coauthors, 2007: Technical summary. *Climate Change 2007: The Physical Science Basis,* S. Solomon et al., Eds., Cambridge University Press, 19–91.

Trenberth, K. E., and Coauthors, 2007: Observations: Surface and atmospheric climate change. *Climate Change 2007: The Physical Science Basis,* S. Solomon et al., Eds., Cambridge University Press, 234–336.

Van den Dool, H. M., and R. M. Chervin, 1986: A comparison of month-to-month persistence of anomalies in a general circulation model and in the earth's atmosphere. *J. Atmos. Sci.,* **43,** 1454–1466.

Wang, W., S. Saha, H.-L. Pan, S. Nadiga, and G. White, 2005: Simulation of ENSO in the new NCEP coupled forecast system model (CFS03). *Mon. Wea. Rev.,* **133,** 1574–1593.